Kinetochores accelerate centrosome separation to ensure faithful chromosome segregation

Nunu Mchedlishvili[1,*], Samuel Wieser[1,2,*], René Holtackers[1], Julien Mouysset[1], Mukta Belwal[1], Ana C. Amaro[1] and Patrick Meraldi[1,‡]

[1]Institute of Biochemistry, ETH Zurich, Schafmattstrasse 18, 8093 Zürich, Switzerland
[2]Wellcome Trust/Cancer Research Gurdon Institute, University of Cambridge, Tennis Court Road, Cambridge CB2 1QN, UK

*These authors contributed equally to this work
‡Author for correspondence (patrick.meraldi@bc.biol.ethz.ch)

Accepted 28 August 2011
Journal of Cell Science 125, 906–918

doi: 10.1242/jcs.091967

Summary

At the onset of mitosis, cells need to break down their nuclear envelope, form a bipolar spindle and attach the chromosomes to microtubules via kinetochores. Previous studies have shown that spindle bipolarization can occur either before or after nuclear envelope breakdown. In the latter case, early kinetochore–microtubule attachments generate pushing forces that accelerate centrosome separation. However, until now, the physiological relevance of this prometaphase kinetochore pushing force was unknown. We investigated the depletion phenotype of the kinetochore protein CENP-L, which we find to be essential for the stability of kinetochore microtubules, for a homogenous poleward microtubule flux rate and for the kinetochore pushing force. Loss of this force in prometaphase not only delays centrosome separation by 5–6 minutes, it also causes massive chromosome alignment and segregation defects due to the formation of syntelic and merotelic kinetochore–microtubule attachments. By contrast, CENP-L depletion has no impact on mitotic progression in cells that have already separated their centrosomes at nuclear envelope breakdown. We propose that the kinetochore pushing force is an essential safety mechanism that favors amphitelic attachments by ensuring that spindle bipolarization occurs before the formation of the majority of kinetochore–microtubule attachments.

Key words: CCAN, Centrosome, Kinetochore, Microtubule poleward flux, Mitosis, Mitotic Spindle

Introduction

Chromosome segregation in somatic animal cells requires the separation of centrosomes to ensure bipolarization of the mitotic spindle (reviewed by Walczak and Heald, 2008; Tanenbaum and Medema, 2010). Spindle bipolarization is promoted by several parallel processes, which provide robustness, including anti-parallel microtubule sliding driven by the kinesins Eg5 and Kif15, chromatin-induced microtubule nucleation, self-assembling properties of mitotic microtubules, and interactions between astral microtubules and the cell cortex. Centrosome separation can occur at two different stages of mitosis: during prophase as centrosomes separate around the nuclear envelope, or during early prometaphase when they are driven apart after nuclear envelope breakdown (NEBD) after forming a transient monopolar spindle (Rattner and Berns, 1976; Aubin et al., 1980; Waters et al., 1993; Rosenblatt, 2005). Centrosome separation during prophase or prometaphase relies on distinct sets of molecular players, indicating that these events are not just separate in time, but represent different functional pathways. The cortical acto-myosin network is only essential for the prometaphase pathway (Rosenblatt et al., 2004), and kinetochore–microtubule attachments accelerate centrosome separation in the prometaphase pathway but have no effect on the separation kinetics in the prophase pathway (Toso et al., 2009). Kinetochores accelerate centrosome separation by promoting plus-end microtubule polymerization, which generates a pushing force that drives the two poles apart (Silk et al., 2009; Toso et al., 2009). Later, when coupled to minus-end depolymerization, the same plus-end polymerization results in poleward microtubule flux (Kwok and Kapoor, 2007). This pushing force is impaired firstly if the rate of plus-end polymerization is reduced, as seen after the depletion of the kinesins Kif2a and MCAK or depletion of centromere-associated protein E (CENP-E); secondly, if kinetochore fibers (k-fibers) are lost after depletion of the NDC80 complex, which is essential for kinetochore–microtubule attachments; or thirdly, if k-fibers are weakened (DeLuca et al., 2002; Ganem and Compton, 2004; Cheeseman and Desai, 2008; Maffini et al., 2009; Toso et al., 2009). Weak k-fibers are observed in cells lacking the kinetochore protein CENP-O, a subunit of the CCAN (constitutive centromere-associated network) kinetochore complex (Toso et al., 2009). The 13-subunit CCAN complex binds and controls the assembly of centromeric nucleosomes, and regulates k-fiber dynamics, thus bridging the DNA and microtubule hemispheres of kinetochores (Okada et al., 2006; Hori et al., 2008; Carroll et al., 2009; Amaro et al., 2010). Interestingly, depletion of various CCAN subunits differentially affects k-fiber dynamics. Disruption of the entire complex, as seen after CENP-H depletion, leads to hyperstable k-fibers and increased microtubule plus-end dynamics at k-fibers (Amaro et al., 2010). The lack of controlled k-fiber dynamics in CENP-H-depleted cells disrupts proper chromosome movements and impairs chromosome alignment on the metaphase plate, but does not affect bipolar spindle formation. By contrast, depletion of the CENP-O complex, which only removes CENP-O, CENP-P,

Journal of Cell Science

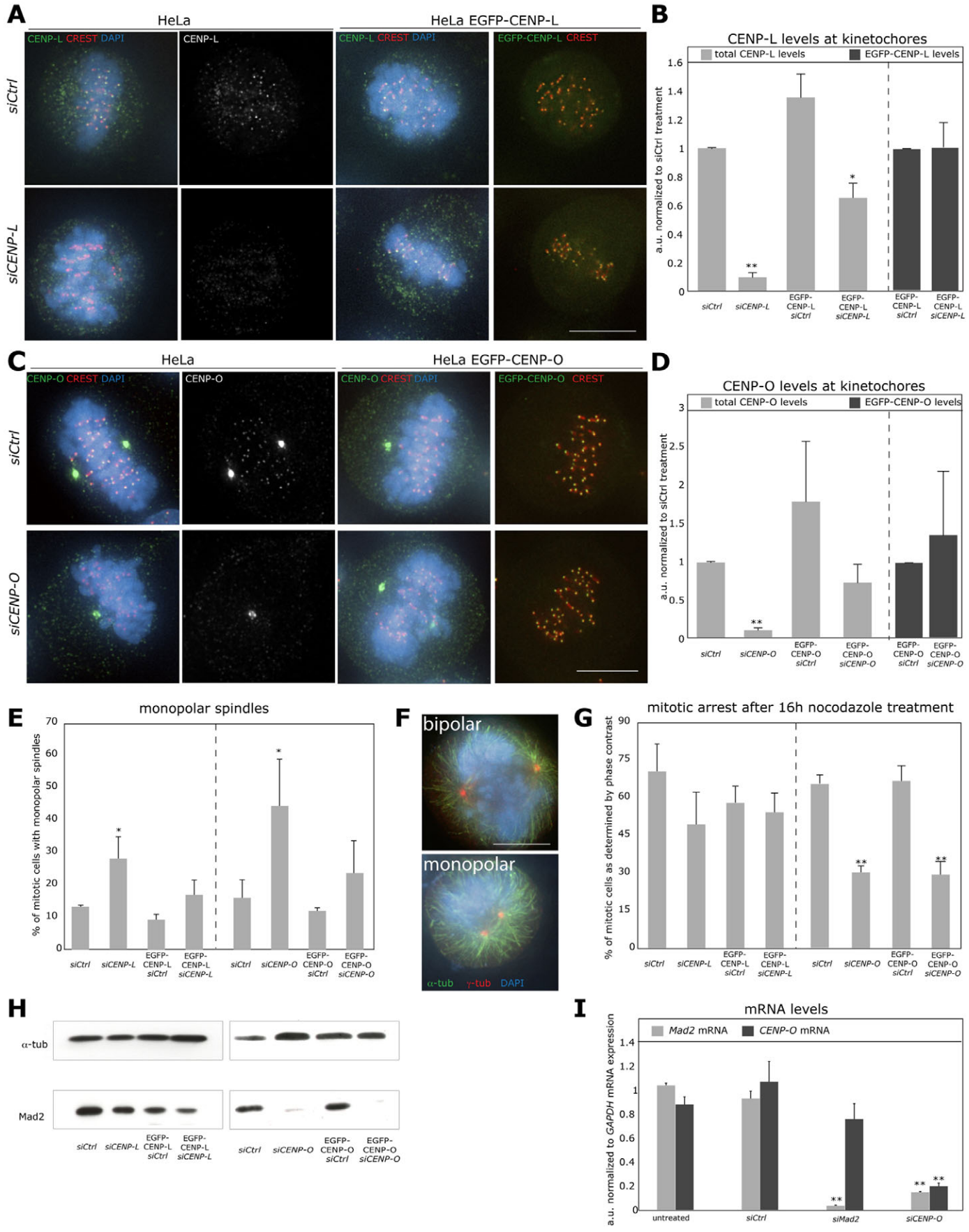

Fig. 1. See next page for legend.

CENP-Q, CENP-U and CENP-R from kinetochores, leads to a partial destabilization of k-fibers and a delay in bipolar spindle formation in the prometaphase pathway (McClelland et al., 2007; Toso et al., 2009).

One key issue is the physiological importance of the kinetochore pushing force on mitotic progression, because its absence only delays centrosome separation in prometaphase by 6–9 minutes (Toso et al., 2009). This question has been difficult to address because all tested perturbations affecting the kinetochore pushing force also impaired chromosome alignment or disrupted the spindle checkpoint (Wood et al., 1997; DeLuca et al., 2002; Ganem and Compton, 2004; Meraldi et al., 2004; McAinsh et al., 2006). One interesting candidate for the study of this problem is depletion of the kinetochore protein CENP-L. This protein is, like CENP-O, a CCAN subunit whose depletion results in an accumulation of monopolar spindles, suggesting that it is crucial for the kinetochore pushing force (McClelland et al., 2007). However, in contrast to CENP-O depletion, CENP-L depletion does not impair the spindle checkpoint (McClelland et al., 2007). Moreover, in terms of kinetochore protein recruitment dependencies, CENP-L has been closely associated to the CCAN subunit CENP-N, which it can bind in vivo, and to the CENP-H, CENP-I and CENP-K subunits, which are all required for the assembly of the entire CCAN complex, rather than to the CENP-O complex (Okada et al., 2006; McClelland et al., 2007; Carroll et al., 2009). We have investigated the CENP-L depletion phenotype in order to study at the cellular level how the loss of the kinetochore pushing force affects chromosome segregation in the prometaphase pathway, and to better understand how different CCAN protein depletions affect k-fiber dynamics.

Fig. 1. CENP-L depletion leads to monopolar spindles, but does not affect the spindle checkpoint. (**A**) Representative images of HeLa and HeLa EGFP–CENP-L cells treated with control or *CENP-L* siRNAs and stained with CENP-L antibodies, CREST antisera (kinetochore marker) and DAPI (DNA marker). (**B**) Determination of CENP-L and EGFP–CENP-L levels on kinetochores by quantitative immunofluorescence based on CENP-L/CREST or EGFP–CENP-L/CREST signal ratios. Quantification is based on three independent experiments with five cells in each experiment and ten kinetochores per cell. (**C**) Representative images of HeLa and HeLa EGFP–CENP-O cells treated with *siCtrl* or *siCENP-O* and stained with CENP-O antibodies, CREST antisera and DAPI. (**D**) Quantification of CENP-O and EGFP–CENP-O levels on kinetochores based on CENP-O/CREST or EGFP–CENP-O/CREST signal ratios. Quantification is based on three independent experiments with five cells in each experiment and ten kinetochores per cell. (**E**) Quantification of the percentage of monopolar spindles in HeLa, HeLa EGFP–CENP-L and HeLa EGFP–CENP-O mitotic cells treated with *siCtrl*, *siCENP-L* or *siCENP-O*. The percentage of monopolar spindles was determined in fixed cells by immunofluorescence ($n \geq 50$ cells per experiment). (**F**) Examples of *siCENP-L*-treated mitotic cells with either bi- or monopolar spindles as quantified in E. Cells were stained with α-tubulin (green; microtubules), γ-tubulin (red; spindle poles) and DAPI (blue; chromosomes). (**G**) Quantification of the spindle checkpoint response in HeLa, HeLa EGFP–CENP-L and HeLa EGFP–CENP-O mitotic cells treated with *siCtrl*, *siCENP-L* or *siCENP-O*. The spindle checkpoint response was determined based on the number of rounded-up mitotic cells found after treatment with 100 ng/ml nocodazole for 16 hours ($n \geq 150$ cells per experiment). (**H**) Immunoblotting of cellular Mad2 levels in HeLa, HeLa EGFP–CENP-L and HeLa EGFP–CENP-O mitotic cells treated with *siCtrl*, *siCENP-L* or *siCENP-O*. Immunoblots against α-tubulin served as loading control. (**I**) Measurement of *Mad2* and *CENP-O* mRNAs by qRT-PCR from cells treated with *siCtrl*, *siCENP-O* or *siMad2*. All errors bars indicate s.e.m. based on at least three independent experiments. $*P<0.05$, $**P<0.01$ compared with corresponding control cells using a *t*-test. Scale bars: 10 μm.

Results

To investigate the phenotype of CENP-L depletion we used polyclonal antibodies raised in rabbits against a CENP-L peptide (Amaro et al., 2010). These antibodies recognized kinetochores by immunofluorescence in dividing HeLa cells, as their signal colocalized with CREST antibodies, which label inner centromeres (Fig. 1A) (Moroi et al., 1980). These kinetochore labels disappeared in cells treated with siRNA targeting CENP-L (*siCENP-L*), indicating that the CENP-L antibodies are specific and that CENP-L depletion is efficient. Fig. 1B shows that there was 10% remaining CENP-L signal at kinetochores compared with cells treated with control (scrambled) siRNA (*siCtrl*). These immunofluorescence data were confirmed by immunoblotting. In total cell extracts, CENP-L antibodies recognized a 39-kDa band that disappeared after treatment with *siCENP-L* (supplementary material Fig. S1). As previously described, treatment with *siCENP-L* or with siRNA against CENP-O (*siCENP-O*) (10% remaining CENP-O signal at kinetochores compared with *siCtrl*-treated cells; Fig. 1C,D) led to a specific accumulation of monopolar spindles in mitotic cells, as measured by immunofluorescence of antibodies to α-tubulin (microtubules) and γ-tubulin (spindle poles), and using DAPI to label chromosomes (Fig. 1E,F) (McClelland et al., 2007). However, in contrast to CENP-O depletion, CENP-L depletion did not significantly weaken the spindle checkpoint response, as cells still arrested in mitosis in the presence of the spindle poison nocodazole (Fig. 1G). We had previously linked this difference to the absence of the spindle checkpoint protein Mad2 at kinetochores in *siCENP-O*-treated cells (McAinsh et al., 2006; McClelland et al., 2007). This difference seemed specific because it was based on two independent siRNAs for each depletion (McAinsh et al., 2006; McClelland et al., 2007); however, recent studies showed that the *Mad2* mRNA is a frequent off-target for various siRNAs, raising the possibility that our siRNAs targeting CENP-O might also target Mad2 (Hubner et al., 2010; Westhorpe et al., 2010). To test for this possibility and to unequivocally confirm the specificity of our phenotypes, we generated stable HeLa cell lines expressing either siRNA-resistant EGFP–CENP-L or siRNA-resistant EGFP–CENP-O. Quantification of immunofluorescence staining with CENP-L or CENP-O antibodies and measurement of EGFP intensities confirmed that the cell lines expressed siRNA-resistant versions of EGFP–CENP-L or EGFP–CENP-O, respectively (Fig. 1A–D). Expression of either siRNA-resistant EGFP–CENP-L or EGFP–CENP-O suppressed the accumulation of monopolar spindles in cells treated with the corresponding siRNA (Fig. 1E). By contrast, expression of EGFP–CENP-O did not rescue the loss of the spindle checkpoint in *siCENP-O* treated cells (Fig. 1G). Immunoblotting showed that CENP-O depletion, but not CENP-L depletion, also resulted in very low cellular Mad2 protein levels, suggesting that *siCENP-O* treatment impairs spindle checkpoint signaling by off-targeting *Mad2* RNA (Fig. 1H). This was confirmed by quantitative RT-PCR measurements, which showed that *siCENP-O* transfection resulted in a severe reduction of both *CENP-O* and *Mad2* mRNA levels (Fig. 1I). We conclude that the monopolar spindle phenotype associated with CENP-O and CENP-L depletions is specific, but that the loss of the spindle

checkpoint in *siCENP-O* treated cells results from an off-target effect.

Loss of CENP-L deregulates k-fiber dynamics

To better understand CENP-L function and the origins of monopolar spindles, we first investigated how CENP-L depletion affects microtubule dynamics, in comparison to the previously published results of CENP-O or CENP-H depletion. For this purpose we quantified the stability of k-fibers by immunofluorescence microscopy using 15 minutes of cold treatment, which is known to depolymerize all the microtubules that are not stably end-on attached to kinetochores (Salmon and Begg, 1980). In late prometaphase or metaphase cells, CENP-L depletion significantly reduced the intensity of k-fibers compared with cells treated with control siRNA, but it did not abolish k-fibers, as seen after the depletion of the NDC80 subunit Nuf2R (Fig. 2A,B) (DeLuca et al., 2002). This indicated a weakening of the k-fibers, a phenotype very similar to that seen after CENP-O

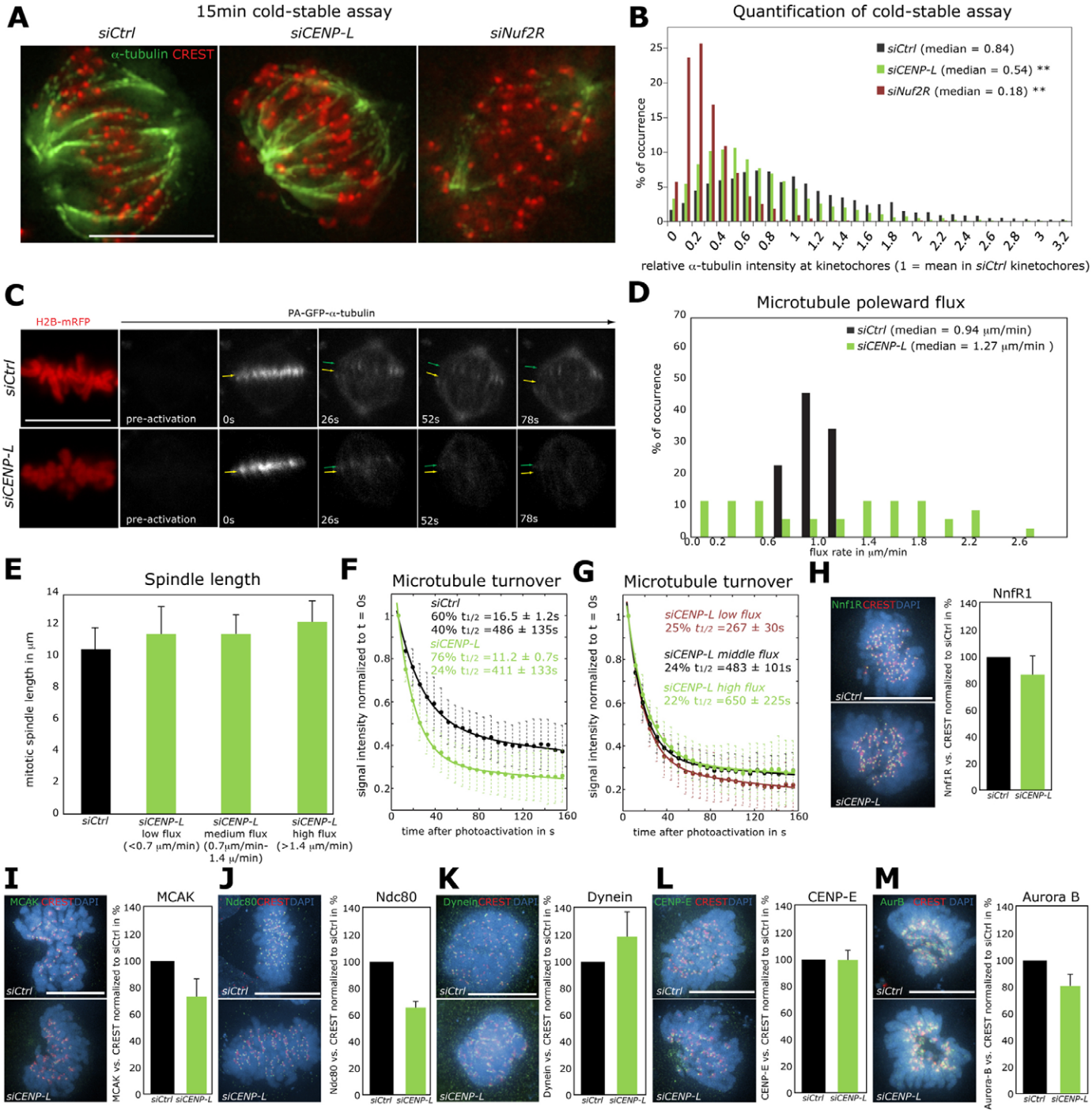

Fig. 2. See next page for legend.

depletion, but opposite to the phenotype seen after loss of CENP-H, which stabilizes k-fibers (Toso et al., 2009; Amaro et al., 2010). In a second assay, we used a HeLa cell line expressing histone H2B–mRFP and photoactivatable (PA-)GFP–α-tubulin to measure the rate of poleward microtubule flux and to measure the tubulin turnover of k-fibers. The H2B signal served as a marker to locate and photoactivate microtubules above the plate in metaphase cells and to follow the progression of the activated tubulin spots towards the spindle poles, which reflect poleward microtubule flux (Fig. 2C). Whereas *siCtrl*-treated cells had a narrow distribution of flux rates with a median of 0.94 μm/minute, *siCENP-L*-treated cells exhibited a very broad range of flux rates (0.2–2.6 μm/minute) with a median of 1.27 μm/minute (Fig. 2D). This broad range of flux rates was very different from the phenotype seen after CENP-H or CENP-O depletion, which either blocked (*siCENP-H*) or slightly accelerated (*siCENP-O)* poleward microtubule flux rate (Toso et al., 2009; Amaro et al., 2010), but did not lead to a highly variable flux rates. Interestingly, CENP-L-depleted cells with low (<0.7 μm/minute), medium (0.7–1.4 μm/minute) or high (>1.4 μm/minute) poleward microtubule flux rates had very similar spindle sizes, indicating that CENP-L-depleted cells adapt to changes in k-fiber dynamics to maintain a constant spindle size (Fig. 2E). Moreover, we noted that CENP-L depletion led to slightly longer spindles compared with controls ($P<0.05$; Fig. 2E), indicating that CENP-L-depleted cells adapt to changes in k-fiber dynamics to maintain a constant spindle size.

To obtain a better description of the inherent dynamics of k-fibers, we next compared the dissipation rate of PA-GFP in control and CENP-L-depleted cells. It has been previously shown that this dissipation rate reveals two populations of microtubules in the spindle: a fast population of free microtubules and a slow population of microtubules in k-fibers (Zhai et al., 1995). By applying a double-exponential fit to the dissipation curve (see Materials and Methods), the half-life of each microtubule population and their relative abundance could be extracted (Fig. 2F). This revealed that control cells contained 60% fast microtubules (half-life of 16.5±1.2 seconds) and 40% slow microtubules (half-life of 486±135 seconds), consistent with previous measurements (Fig. 2F) (Zhai et al., 1995; Bakhoum et al., 2009). By contrast, CENP-L-depleted cells contained a much smaller proportion of slow microtubules (24%), consistent with our measurements in the cold-stable assay, but did not strongly affect the half-life of either fast (11.2±0.7 seconds) or slow (411±133 seconds) microtubules (Fig. 2F).

Given the large variation in the rate of poleward microtubule flux, we then tested whether the turnover of k-fibers was different in cells with low flux rate (<0.7 μm/minute), medium flux rate (0.7–1.4 μm/minute) or high flux rate (>1.4 μm/minute). We found that all three populations had a similar small proportion of slow microtubules (25, 24 and 22%, respectively; Fig. 2G), but that cells with higher flux rate also had longer k-fiber half-lives (267±30, 483±101 and 650±225 seconds, respectively; Fig. 2G). The uniform reduction in the abundance of microtubules with a slow turnover implied similar CENP-L depletion levels in all three populations, indicating that the cell-to-cell variation in poleward microtubule flux rate and k-fiber turnover is a genuine consequence of CENP-L depletion and is not caused by varying depletion levels. Moreover, our results suggest that a higher flux rate leads to a higher microtubule half-life.

What are the molecular mechanisms by which CENP-L depletion affects k-fiber dynamics? Our previous experiments suggested that CENP-L depletion affects k-fiber dynamics because of an imbalance within the CCAN complex, but other non-CCAN-related factors had not been excluded (McClelland et al., 2007). To test this hypothesis, we used quantitative immunofluorescence to analyze the composition of mitotic kinetochores in CENP-L-depleted cells and in control cells. This analysis revealed (data not shown), as previously published (McClelland et al., 2007), that CENP-L depletion abolished the binding of CENP-O to kinetochores and severely restricted the binding of more inner CCAN components such as CENP-I. In contrast to those changes in the CCAN composition, CENP-L depletion did not or only weakly affected the recruitment of other key kinetochore components such as Nnf1R (MIND complex component), Hec1/Ndc80 (NDC80 complex), the microtubule motor proteins CENP-E and dynein, the protein kinase Aurora B and the kinesin-13 MCAK, which acts as a microtubule depolymerase at kinetochores (Fig. 2H–M) (Cheeseman and Desai, 2008; Kops et al., 2010). We conclude that CENP-L

Fig. 2. Loss of CENP-L weakens k-fibers and deregulates poleward microtubule flux. (**A**) Representative immunofluorescence images of HeLa cells that were treated with *siCtrl*, *siCENP-L* and *siNuf2R*, subjected to 15 minutes of cold treatment on ice, fixed and stained by immunofluorescence with antibodies against α-tubulin (green) and CREST (red). (**B**) Quantification of α-tubulin intensities in the vicinity of kinetochores in *siCtrl*-, *siCENP-L*- or *siNuf2R*-treated cells as indicated in the Materials and Methods. Shown are the distributions of tubulin intensities for all kinetochores in three independent experiments with over 3000 kinetochores (*siCtrl* and *siCENP-L*) or one independent experiment with 750 kinetochores (*siNuf2R)*. $^{**}P<0.001$ compared with control according to the Mann–Whitney test. (**C**) Successive frames before and after photoactivation of stable PA-GFP–α-tubulin/H2B–mRFP HeLa cells treated with *siCtrl* or *siCENP-L*. PA-GFP–α-tubulin fluorescence was activated along a stripe parallel and next to the metaphase plate. An H2B–mRFP (DNA) frame is shown for the first time point of the live-cell movie after activation. The yellow arrows indicate the position of the initial photoactivation, the green arrows mark the progression of the photoactivation mark. In cases where the turnover was rapid, as in the example of a *siCENP-L*-treated cell, the flux rate could only be followed for 1 minute. (**D**) Quantification of poleward microtubule flux rates in cells treated with *siCtrl* ($n=11$ cells) or *siCENP-L* ($n=36$ cells). (**E**) Spindle length (pole–pole distance) in control ($n=11$ cells) and CENP-L-depleted cells as measured from photoactivation experiments. CENP-L-depleted cells were segmented in cells with low flux ($n=12$ cells), medium flux ($n=9$ cells) and high flux rate ($n=15$ cells). Error bars indicate s.d. **(F)** Quantification of fluorescence intensity decay of the photoactivated regions over time in control ($n=11$ cells) and CENP-L-depleted ($n=36$ cells) cells. The lines through the data points were fitted to a double-exponential equation corresponding to slow and fast microtubule populations (see Materials and Methods). Indicated are the half-lives of the populations and their relative abundance. Error bars indicated cell-to-cell s.d. (**G**) The data points of CENP-L-depleted cells were further segmented in a population with low, medium or high flux rate and subjected to the same analysis as in F ($R^2>0.99$ in all cases). (**H–M**) Representative images of *siCtrl*- and *siCENP-L*-treated cells stained with CREST antisera (red), DAPI (blue) and antibodies against Nnf1R (H), MCAK (I), Ndc80 (J), Dynein intermediate chain (K), CENP-E (L) and Aurora B (M) (all in green). The relative abundance of each protein was quantified as a ratio to the CREST signal and normalized to the *siCtrl*-treated cells (quantification panels). Note that the Dynein intermediate chain signal was quantified in nocodazole-treated cells because dynein only binds to unattached kinetochores. The quantifications are based on two separate experiments with five cells and ten kinetochores per cell measured. Error bars indicate s.e.m. Scale bars: 10 μm.

depletion probably affects k-fiber dynamics through a deregulation of CCAN and not by affecting the recruitment of other kinetochore proteins previously implicated in this process (see Discussion).

CENP-L depletion impairs the regularity of chromosome movements

One crucial output of k-fiber dynamics is the movement of sister-kinetochores around the metaphase plate, which oscillate in a semi-regular manner along the spindle axis (Jaqaman et al., 2010). Using a kinetochore tracking assay we have previously shown that the regularity of these oscillations can be quantified using an autocorrelation analysis: this yields a curve, in which the first negative lobe indicates the average half-period of the oscillator, and the depth reflects the regularity of the oscillations (Fig. 3A) (Jaqaman et al., 2010). Whereas the analysis of cells treated with control siRNA yielded an autocorrelation curve with a first minimum of –0.33 at 42.5 seconds, the autocorrelation curve for CENP-L-depleted cells was nearly flat (Fig. 3A). However, it did not overlap with the curves seen after a complete disruption of sister-kinetochore oscillations, such as in fixed cells (Fig. 3A), CENP-H-depleted cells (abrogation of CCAN, data not shown) (Amaro et al., 2010) or Nuf2R-depleted cells (abrogation of NDC80 complex, data not shown) (Jaqaman et al., 2010), indicating the remaining presence of oscillations with a minimal regularity in CENP-L-depleted cells. The kinetochore tracking assay further revealed that CENP-L-depleted metaphase cells had significantly shorter interkinetochore distances ($P<0.001$ in Mann–Whitney test) and slower sister-kinetochore movements ($P<0.001$ in Mann–Whitney test) than control cells (Fig. 3B,C). This confirmed a weakening of the k-fibers and suggested a reduction in the forces acting on sister-kinetochore pairs. Overall, the severe reduction in the regularity of metaphase chromosome movements confirmed the deregulation of kinetochore–microtubule dynamics in CENP-L-depleted cells. This raised the issue of whether CENP-L depletion might not only affect centrosome separation, but also affect chromosome alignment.

CENP-L depletion specifically disrupts chromosome segregation in the prometaphase pathway

To investigate the functional consequence of CENP-L depletion on centrosome separation and chromosome segregation, we used time-lapse imaging of dividing HeLa cells expressing H2B–mCherry and mEGFP–α-tubulin (Fig. 4A) (Steigemann et al., 2009). Cells were assigned either to the prophase pathway if their centrosomes were separated on opposite side of the nucleus at NEBD (about 50% of the cells), or to the prometaphase pathway if both centrosomes were located on the same side of the chromatin (Fig. 4A,B; supplementary material Movies 1 and 2). Using NEBD as $t=0$, we monitored the timing of centrosome separation, chromosome alignment and anaphase onset, as well as the rate of chromosome segregation errors (Fig. 4C–F). In CENP-L-depleted cells we observed an average delay in centrosome separation of 5.8 minutes for cells using the prometaphase pathway ($P<0.01$ in Mann–Whitney test; Fig. 4C), indicating that CENP-L depletion abrogated the kinetochore-pushing force to the same extent as CENP-O or Nuf2R depletion (Toso et al., 2009). Compared with *siCtrl* treatment, CENP-L depletion led to a 17.7 minute delay in chromosome alignment and a 22.2 minute delay in anaphase onset in cells using the prometaphase pathway ($P<0.01$ in Mann–Whitney test; Fig. 4D,E). The delay in anaphase onset always correlated with the presence of unaligned chromosomes that eventually congressed to the metaphase plate, implying that unaligned chromosomes were the major cause of anaphase delay. Cells in the prometaphase pathway were not only slower in their mitotic progression, they also displayed a threefold increase in the rate of chromosome segregation errors (44% versus 16% in control cells, $P<0.01$ in Mann–Whitney test; Fig. 4F). By contrast, CENP-L-depleted cells using the prophase pathway had normal timings for centrosome separation, chromosome

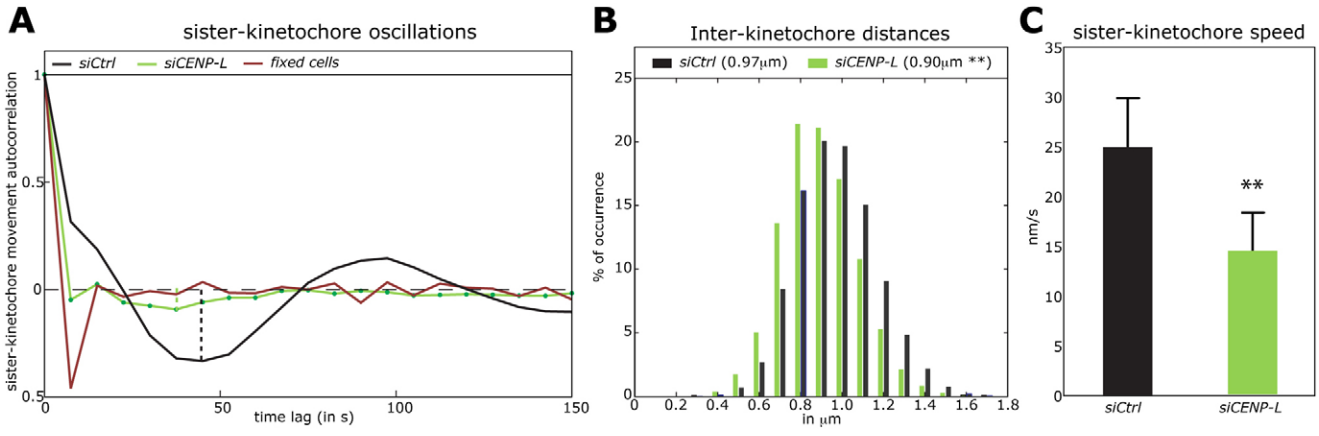

Fig. 3. CENP-L depletion impairs chromosome oscillation regularity. (**A**) Autocorrelation function of translational sister-kinetochore movements along the spindle axis (kinetochore oscillation) of *siCtrl*-treated, *siCENP-L*-treated or fixed cells. The autocorrelation function was calculated by combining all aligned sister-kinetochore pairs for each condition. The first negative lobe in control cells (dotted line) indicates the half-period of the mean oscillation period, and its depth indicates the oscillation regularity. Note that a random motion always produces a negative value at the first lag (Jaqaman et al., 2010). (**B**) Distribution of interkinetochore distances in *siCtrl*- or *siCENP-L*-treated cells, as measured by the kinetochore tracking assay. Numbers in brackets indicate the mean inter-kinetochore distances. (**C**) Average sister-kinetochore pair speed along the spindle axis of *siCtrl*- or *siCENP-L*-treated cells. Error bars indicate s.d. representing cell-to-cell variation. $^{**}P<0.001$ compared with control, according to the Mann–Whitney test.

alignment and anaphase onset, and normal segregation error rates compared with control cells (Fig. 4C–F). This indicated that CENP-L depletion led to severe chromosome segregation defects both in timing and accuracy that were specific to the prometaphase pathway.

The absence of any visible defect in CENP-L-depleted cells using the prophase pathway was surprising because this depletion deregulates k-fiber stability, microtubule flux and metaphase chromosome movements. Indeed, abrogation of chromosome oscillations in CENP-H-depleted cells correlates with a widening of the metaphase plate and defects in chromosome alignment, suggesting that chromosome oscillations play an important role in the formation of a tight metaphase plate (Amaro et al., 2010). By contrast, CENP-L-depleted cells displayed metaphase plate widths that were on average 20% tighter than in *siCtrl*-treated cells ($P<0.01$, Mann–Whitney test), indicating an excellent ability to align chromosomes despite a strong deregulation of the regularity of kinetochore movements (Fig. 4G).

CENP-L depletion in the prometaphase pathway results in syntelic and merotelic attachments

The absence of chromosome segregation defects in CENP-L-depleted cells using the prophase pathway indicates that a 5–6 minute delay in centrosome separation during prometaphase is sufficient to cause long delays in chromosome alignment and severe chromosome segregation errors. What could be the cause of this nonlinear response? One hypothesis is that the prolonged presence of a transient monopolar spindle in CENP-L-depleted cells using the prometaphase pathway favors the formation of syntelic (both kinetochores attached to the same pole) or merotelic (one kinetochore bound to both spindle poles) kinetochore–microtubule attachments, as seen after the formation of permanent monopolar spindles (Lampson et al., 2004). Whereas syntelic attachments impair chromosome alignment and delay anaphase onset if they are not corrected, merotelic attachments are not detected by the spindle checkpoint and often result in chromosome segregation errors, mostly lagging chromosomes (Cimini et al., 2001). To corroborate this hypothesis, we evaluated the attachment status of unaligned sister-kinetochore pairs in CENP-L-depleted cells by immunofluorescence. HeLa cells were cold-treated (7 minutes), to remove most of the spindle microtubules and then stained for kinetochore-microtubules with α-tubulin antibodies (microtubules) and CREST antisera (kinetochores). Although a visual inspection indeed revealed the presence of syntelic attachments in the vicinity of the poles in CENP-L-depleted cells (Fig. 5A), a more quantitative analysis of the attachment status was hindered by the high density of the microtubule network proximal to spindle poles. Therefore, to better quantify syntelic attachments, we stained stable cell lines expressing both a marker for spindle poles (EGFP–centrin1) and a marker for kinetochores (EGFP–CENP-A) for CREST and DAPI to measure for each sister-kinetochore pair the angle between the vector connecting both sister-kinetochores and the vector connecting the center of mass of both sister-kinetochores to the closest spindle pole (Fig. 5B,C). Whereas syntely is expected to give an angle of about 80–90° (both kinetochores facing the spindle poles), monotelic (one sister-kinetochore attached), amphitelic or laterally attached sister-kinetochores should result in much smaller angles. Consistent with this hypothesis, we found that the axes connecting aligned, amphitelic sister-kinetochores in *siCENP-L*- or *siCtrl*-treated cells (median of 33° and 31°, respectively), or the axes of most unaligned sister-kinetochores in control cells (median 36°) were mostly directed towards the spindle pole (Fig. 5D, left panel). By contrast, the axes of unaligned sister-kinetochores in CENP-L-depleted cells (median 56°) displayed the same distribution of high, perpendicular angles towards the spindle pole as seen with syntelic sister-kinetochores in permanent monopolar spindles induced with the Eg5 inhibitor monastrol (median 58°; Fig. 5D, right panel) (Lampson et al., 2004). We conclude that, in contrast to control cells, most unaligned sister-kinetochores in CENP-L-depleted cells are syntelic. Our immunofluorescence analysis of cold-treated *siCENP-L* cells also revealed the presence of merotelic attachments, in both prometaphase and anaphase cells; however, as for the syntelic attachments, a more precise quantification was hindered by the high density of spindle microtubules (Fig. 5E).

A second key characteristic of merotelic attachments is that such a configuration results in lagging chromosomes in anaphase, which are left behind between the two separating DNA masses (Cimini et al., 2001). Analysis of our live-cell imaging sequences from CENP-L-depleted cells indicated that 85% of the chromosome segregation errors in cells using the prometaphase pathway were due to lagging chromosomes; the other 15% were due to DNA bridges (Fig. 5F). By contrast, in CENP-L-depleted cells using the prophase pathway, only 56% of the chromosome segregation errors were due to lagging chromosomes and 46% to DNA bridges (Fig. 5F). We conclude that CENP-L depletion increases the rate of chromosome segregation errors by causing an accumulation of merotelic kinetochore–microtubule attachments that are not detected by the spindle checkpoint.

Discussion

Here, we have addressed the importance of the kinetochore pushing force, which accelerates centrosome separation in cells that have not yet separated their centrosomes at NEBD. We find that a rapid separation of the two spindle poles is essential for faithful chromosome segregation in the prometaphase pathway. Using the depletion of the CCAN protein CENP-L we show that even a modest delay in centrosome separation (15 instead of 9 minutes) causes severe defects in chromosome alignment and chromosome segregation in this pathway. Our data imply that these defects arise as a consequence of prolonged monopolar spindles, which favor the formation of syntelic and merotelic attachments, most probably due to the many kinetochore–microtubule attachments formed 9–15 minutes after NEBD. Syntelic attachments lead to chromosome alignment defects that will activate the spindle checkpoint and delay anaphase onset, when Aurora B transforms syntelic attachments into monotelic attachments, consistent with our live-cell imaging observations (Tanaka et al., 2002; Hauf et al., 2003; Lampson et al., 2004). By contrast, merotelic sister-kinetochore attachments will not activate the checkpoint, making them the primary source of chromosomal instability during cell division (Cimini et al., 2001). Under normal conditions merotelic attachments are corrected both before and during anaphase in an MCAK- and Aurora-B-dependent manner. However, if too many merotelic attachments arise, the correction machinery will be saturated and cause severe chromosome segregation errors (Cimini et al., 2003; Kline-Smith et al., 2004; Lan et al., 2004; Knowlton et al., 2006). Previous studies have shown that an excess of merotelic attachments can arise in cells with

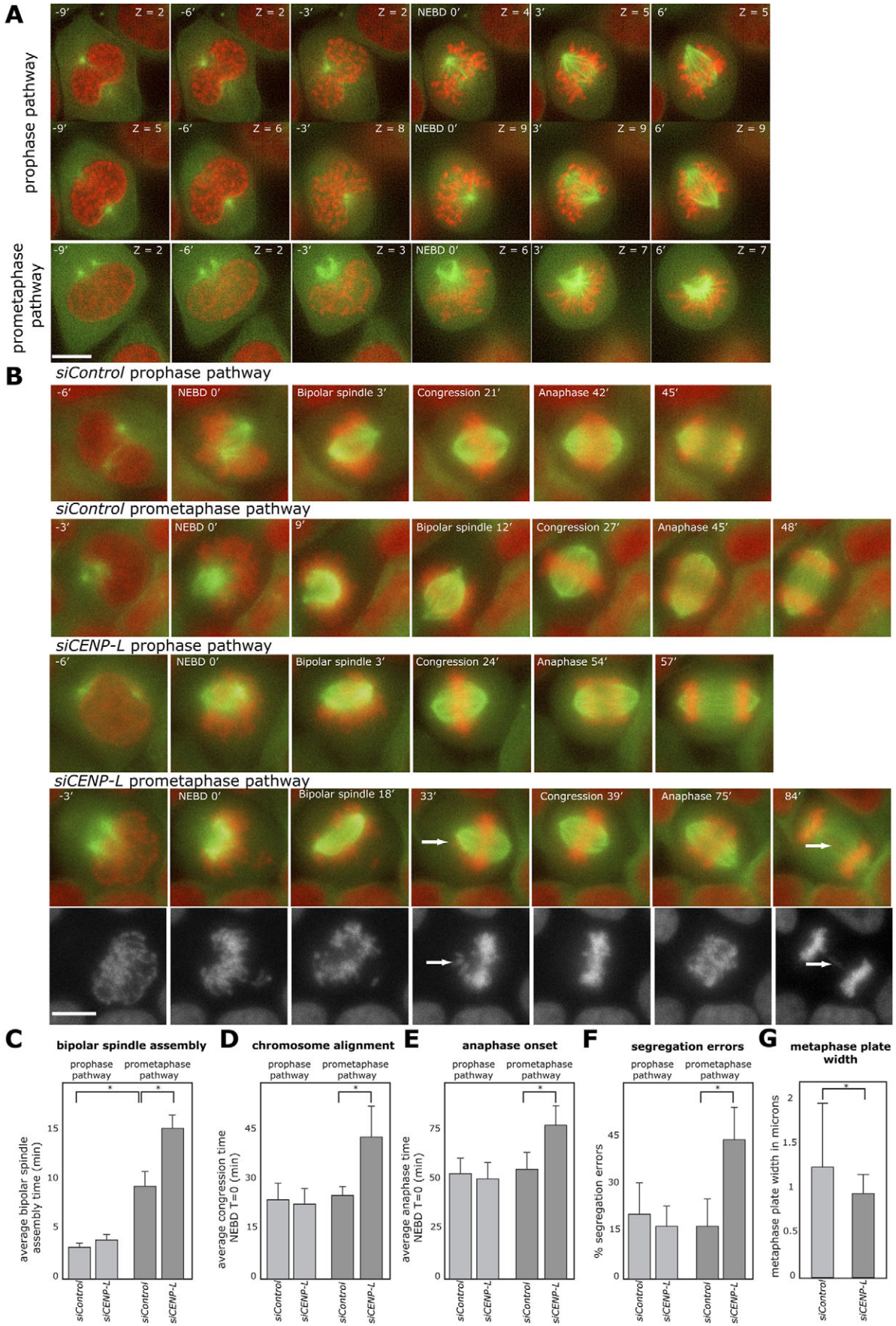

Fig. 4. See next page for legend.

supernumerary centrosomes, which initially form tetrapolar spindles before coalescing into a bipolar configuration; a phenomenon that has been linked to chromosomal instability in cancer cells (Ganem et al., 2009; Silkworth et al., 2009). Here, we show that a minor delay in centrosome separation in the prometaphase pathway causes the same phenotype, suggesting that this pathway is not robust and that it could contribute to chromosomal instability during tumorigenesis because both transformed and nontransformed cells use the pro- and prometaphase pathways in similar proportions (Toso et al., 2009). Therefore, one crucial future issue will be to test the robustness of the prometaphase pathway in animals, in the context of three-dimensional tissue with its many external cues that can influence spindle formation.

Another important question is why the prometaphase pathway exists in the first place, as opposed to cell divisions that would rely purely on a separation of the centrosomes before NEBD. It is possible to abolish the prometaphase pathway by depleting the Rootletin protein, which links the two centrosomes until shortly before NEBD (Bahe et al., 2005; Toso et al., 2009). Rootletin depletion has no visible effect on mitotic progression or on the fidelity of chromosome segregation, indicating that the prometaphase pathway is not essential for cell division (data not shown). These observations are consistent with the fact that Rootletin knockout mice are viable, assuming a similar suppression of the prometaphase pathway in mice (Yang et al., 2005). However, Rootletin-deficient mice suffer over time from unstable ciliae, leading to blindness (ciliae defects in photoreceptors) and lung infections (defective mucocilliary clearance), indicating that this protein is essential for the long-term stability of ciliae (Yang et al., 2005). We therefore speculate that the prometaphase pathway is an evolutionary compromise between robust ciliae, which need a solid connection between the two centrosomes, and the need for a rapid centrosome separation at the onset of mitosis. Because cells will not always be able to disrupt the strong connection between the centrosomes in time, they use the kinetochore-pushing force to ensure a rapid bipolarization.

Characterization of the CENP-L depletion phenotype yielded a better insight into the function of the CCAN complex. We had previously postulated that the CCAN complex is composed of two layers of proteins that can mutually control or antagonize each other: a distal layer composed of the CENP-O (CENP-O, CENP-P, CENP-Q, CENP-U and CENP-R) complex and a more proximal layer consisting of all other CCAN proteins (McClelland et al., 2007). CENP-L depletion results in kinetochores lacking any CENP-O complex, very low levels of the other proximal CCAN proteins (such as CENP-H, CENP-K, CENP-I, CENP-M or CENP-N) in these studies (Okada et al., 2006; McClelland et al., 2007) and a strong reduction in k-fiber stability. One cannot exclude the possibility that this lower k-fiber stability is due to the reduced levels (60%) of Ndc80 at kinetochores, a protein that plays a key role in microtubule attachment (Cheeseman and Desai, 2008). However, we note that CENP-H-depleted cells, which do not bind CENP-L at kinetochores, have equally low levels of Ndc80 and yet have hyperstable k-fibers (Amaro et al., 2010). Conversely, cells without a CENP-O complex (CENP-O or CENP-U depletion) have elevated levels of Ndc80 and still they show the same low stability of k-fibers as CENP-L-depleted cells (McClelland et al., 2007; Toso et al., 2009; Hua et al., 2011). The lack of a correlation between Ndc80 levels and k-fiber stability in CCAN protein depletions suggests that the reduction in k-fiber stability in CENP-L-depleted cells is not caused by changes in Ndc80 levels, but rather due to the absence of the CENP-O complex. Moreover, these results confirm our hypothesis that the CCAN complex consists of at least two functional layers that control k-fiber stability.

A second key feature of CENP-L-depleted cells is that their k-fibers still turn over slowly, in contrast to CENP-H-depleted cells, which have a microtubule plus-end turnover that is fast and indistinguishable from that of free spindle microtubules (Amaro et al., 2010). This indicates that the proximal CCAN proteins are required for the reduction in microtubule plus-end turnover and that they can carry out this function even when present at very low levels. The third very striking aspect of microtubule dynamics in CENP-L-depleted cells is their wide range of poleward microtubule flux rates. This is a unique phenotype that is not seen with any other of the other kinetochore protein depletions, which homogeneously accelerate or decrease the rate of flux (Maiato et al., 2003; DeLuca et al., 2006; Maffini et al., 2009; Toso et al., 2009; Amaro et al., 2010). This suggests that CENP-L levels and/or normal CENP-H, CENP-K, CENP-I, CENP-N and CENP-M levels impose a homogenous rate of poleward microtubule flux. If kinetochores lack this imposed regulation, the k-fibers flux with highly variable rates. Finally, as a fourth point, we find that CENP-L depletion severely impairs the regularity of chromosome movements. Because CENP-L did not affect the kinetochore-binding of Aurora B, MCAK, CENP-E or dynein, which are all implicated in chromosome movement (Kops et al., 2010), we conclude that this defect is most probably due to a deregulation of CCAN. Overall, these results validate the emerging view of the CCAN complex as a key regulator of microtubule stability, dynamics and flux rate. We propose that the concentration of these activities in one complex facilitates a gradual balance and adaptation of k-fiber dynamics as cells

Fig. 4. CENP-L depletion disrupts chromosome segregation only in the prometaphase pathway. (**A**) Successive frames from live-cell imaging of untreated HeLa cells expressing H2B–mCherry (red) and α-tubulin–mEGFP (green; to mark chromosomes and microtubules) using either the prophase or the prometaphase pathway. Shown are the positions of the spindle poles before and after NEBD in single z-stacks. Times are indicated using NEBD as $t=0$, stack numbers are indicated as z-number (distance between z-stacks is 1 μm). Note how in the prometaphase cells the two spindle poles are present in the same focal plane, confirming that they are on the same side of the chromatin. (**B**) Successive frames from live-cell imaging of HeLa cells expressing H2B–mCherry (red) and α-tubulin–EGFP (green; to mark chromosomes and microtubules) treated with *siCtrl* or *siCENP-L*. The cells are shown as projection of z-stacks and they follow the prophase or the prometaphase pathway. Indicated are the times of NEBD, congression and anaphase onset. To better visualize unaligned chromosomes (Congression 24′) and the lagging chromosome in late anaphase (84′) of *siCENP-L*-treated cells in the prometaphase pathway (white arrows), separate black and white frames of only H2B–mCherry are shown in the bottom row. Scale bar: 10 μm. (**C**) Average bipolar spindle assembly time, (**D**) average congression time and (**E**) average anaphase onset time after NEBD in *siCtrl*- or *siCENP-L*-treated cells using the pro- or prometaphase pathway. (**F**) Average rate of chromosome segregation errors in *siCtrl*- or *siCENP-L*-treated cells using the pro- or prometaphase pathway. (**G**) Average metaphase plate width in *siCtrl*- or *siCENP-L*-treated cells as determined with the kinetochore tracking assay. All experiments are based on at least three independent experiments. Error bars indicate s.e.m. $*P<0.01$ according to the Mann–Whitney test.

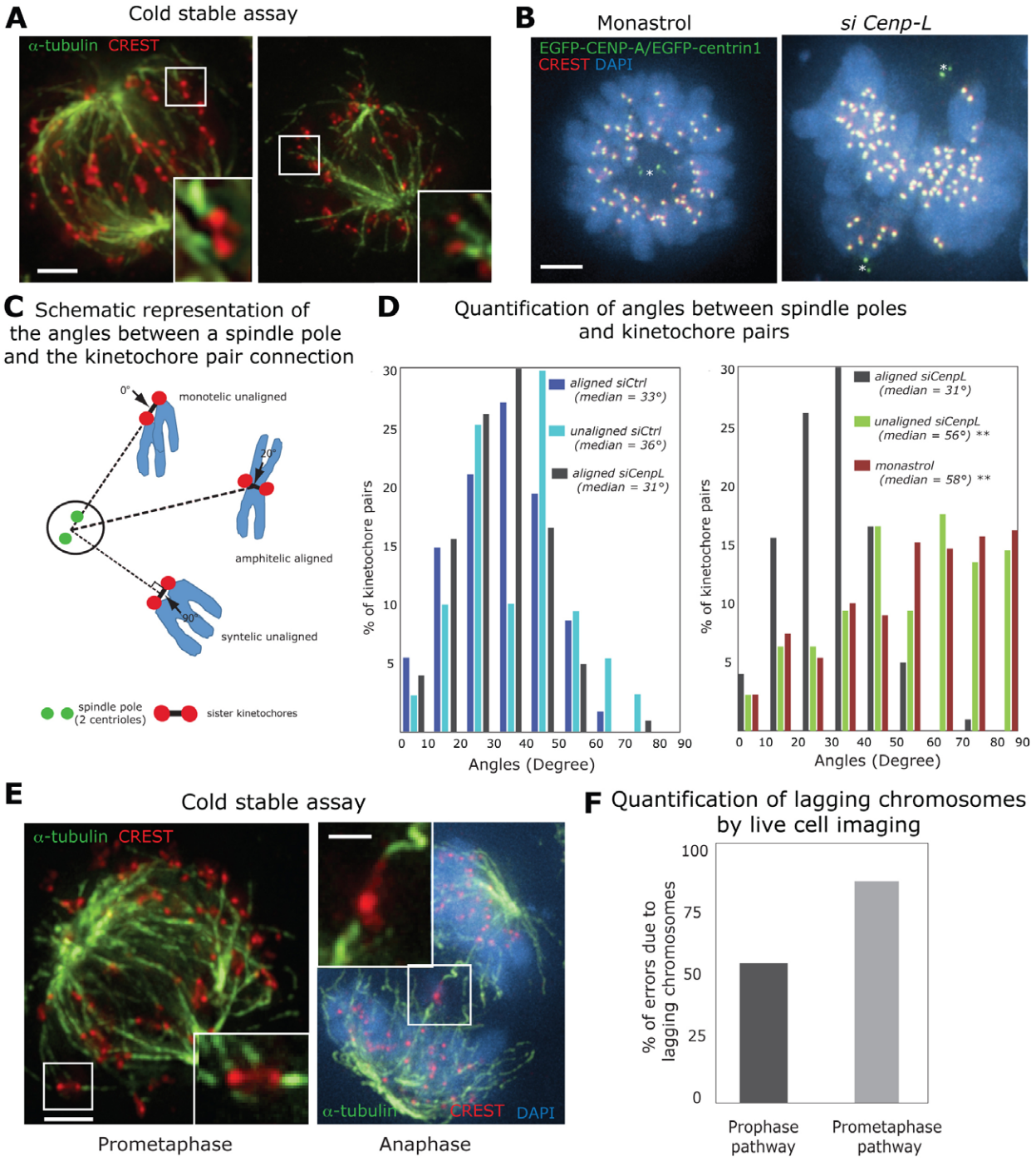

Fig. 5. CENP-L depletion in the prometaphase pathway results in syntelic and merotelic attachments. (**A**) Representative immunofluorescence images of *siCENP-L*-treated HeLa cells with syntelic attachments. Cells were subjected to 7 minutes of cold treatment on ice and stained by immunofluorescence with antibodies against α-tubulin (green) and CREST (red). The insets show higher magnification examples of syntelic attachments. (**B**) Representative immunofluorescence images of HeLa EGFP–CENP-A/EGFP–centrin1 (kinetochore and spindle pole markers, respectively) cells that were treated with *siCENP-L* and the Eg5 inhibitor monastrol and stained with CREST antisera (kinetochores) and DAPI (chromosomes). The spindle poles are indicated with a white asterisk. (**C**) Representation of the measurements of the angle between spindle poles and the connection between kinetochore pairs in syntelic, monotelic and amphitelic sister-kinetochore pairs. (**D**) Quantification of the angle between spindle poles and sister kinetochores. Distributions are based on two independent experiments (*siCtrl* treatment, $n=24$ cells and 200 kinetochore pairs; *siCENP-L* treatment, $n=30$ cells and >200 sister-kinetochore pairs; Monastrol treatment, $n=10$ cells and 200 sister-kinetochore pairs). $^{**}P<0.01$ compared with aligned kinetochore pairs, according to the Mann–Whitney test (**E**) Representative immunofluorescence images of *siCENP-L*-treated HeLa cells with merotelic attachments in prometaphase (left) and anaphase (right). Cells were subjected to 7 minutes of cold treatment on ice and stained by immunofluorescence with antibodies against α-tubulin (green) and CREST (red) and DAPI (blue; chromosomes). Insets show higher magnification examples of merotelic attachments. (**F**) Quantification of the percentage of chromosome segregation errors due to lagging chromosomes in *siCENP-L*-treated cells using either the prophase or prometaphase pathway, based on the live-cell imaging experiments described in Fig. 4. Scale bars: 1 µm.

progress through mitosis (Zhai et al., 1995) and that it would complement other regulatory elements such as Aurora B and astrin (Manning et al., 2010; Schmidt et al., 2010).

In addition to these CCAN-specific insights, we can draw two important general conclusions about the dynamics of the mitotic spindle: First, despite the high variation in flux rates, all CENP-L-depleted cells have similar spindle lengths, indicating that cells tightly coordinate and adapt the rate of minus-end depolymerization and plus-end of depolymerization within k-fibers (any difference between the two rates would change spindle length). Such coordination indicates a mechanical coupling between both ends of the k-fiber, and future research will have to uncover the molecular mechanisms governing this coordination. We can already predict that the rate is governed at the k-fiber plus-end in a CCAN-dependent manner, and we propose that in the absence of such a control at kinetochores, the rate of flux is set more randomly, possibly from the minus-end. Such a mechanism would explain the high cell-to-cell variability but low variability within a particular cell. A second general conclusion is that the rates of poleward microtubule flux correlate with the kinetochore–microtubule half-life. This implies that in the same 'genetic' background a faster incorporation of tubulin subunits at the microtubule plus-end prevents microtubule catastrophe, thus leading to higher half-lives.

The third key result of our CENP-L depletion study is that despite a near loss of regularity in sister-kinetochore oscillations, a weakening of k-fibers and a deregulation of poleward microtubule flux, cells still efficiently align the chromosomes on a metaphase plate if the two centrosomes are separated at NEBD. Note that 50% of HeLa cells use the prophase pathway and that all 51 CENP-L-depleted cells analyzed in the kinetochore tracking assay showed only minimal sister-kinetochore oscillation regularity when analyzed at the single cell level (data not shown). This stands in contrast to the previous observation that a complete loss of sister-kinetochore oscillations correlates with much wider metaphase plates in cells depleted of the CCAN subunit CENP-H (Amaro et al., 2010). Such a difference could indicate that semiregular chromosome oscillations are just a reflection of k-fiber dynamics that do not contribute to the formation of a metaphase plate, or that in the presence of minimally regular sister-kinetochore oscillations chromosome alignment is robust enough to assemble a tight metaphase plate. Possible contributors to such robustness could be the polar ejection force, and the activities of the kinesin-8, Kif18A, and the kinesin-5, CENP-E, which all contribute to chromosome alignment (Rieder et al., 1986; Schaar et al., 1997; Wood et al., 1997; Kapoor et al., 2006; Stumpff et al., 2008). Consistent with this idea, sister-kinetochores can align on an unstable metaphase plate in the absence of bipolar end-on kinetochore attachments (Cai et al., 2009). Therefore, we conclude that under conditions of rapid bipolarization, a minimal regularity of sister-kinetochore oscillations and partial deregulation of kinetochore–microtubule dynamics is compatible with efficient chromosome alignment. However, when cells do not immediately establish a bipolar spindle, a precise regulation of microtubule dynamics and chromosome movements becomes essential.

Materials and Methods

Cell culture, siRNA transfection and drug treatments

HeLa cells were grown in Dulbecco's modified Eagle's medium (DMEM) containing 10% FCS, 100 U/ml penicillin and 100 µg/ml streptomycin at 37℃ with 5% CO_2 in a humidified incubator. The HeLa EGFP–CENP-A, H2B–mCherry/mEGFP–α-tubulin and HPA-GFP–α-tubulin/H2B–mRFP stable cell lines were grown as described (Steigemann et al., 2009; Amaro et al., 2010). HeLa EGFP–CENP-O and EGFP–CENP-L stable cell lines were obtained after transfection with FUGENE6 (Roche) of a pIRES-EGFP–CENP-Opuro or pIRES-EGFP–CENP-Lpuro construct, respectively (obtained by cloning EGFP–CENP-O or EGFP–CENP-L into a pIRESpuro2 vector from Clontech). Stable cloned cell lines were selected in the presence of 500 ng/ml puromycin. To obtain HeLa EGFP–CENP-A/EGFP–centrin1 cells, HeLa EGFP–CENP-A cells were transfected with a pSV40-EGFP–centrin2-IRESneo construct using FUGENE6 (Roche), and stable cloned cell lines were selected in the presence of 1 mg/ml G418. Control (scrambled, 5′-GGACCTGGAGGTCTGCTGT-3′), *Nuf2R* (Meraldi et al., 2004), *Mad2* (Meraldi et al., 2004), *CENP-O* (McClelland et al., 2007) and *CENP-L* siRNAs (5′-CCAUUAUGUGGCUACUACUGAAUUU-3′ for all experiments; the most crucial experiments were repeated and confirmed with a second CENP-L oligonucleotide 5′-UUGAAACACGAACUAAUCUUGUGGC-3′; all from Qiagen) were transfected as described and analysed 48 hours after transfection (Elbashir et al., 2001). For the spindle checkpoint assay, cells were treated for 16 hours with 100 ng/ml of nocodazole. The percentage of mitotic cells was determined via cell rounding by phase-contrast microscopy. The Eg5 inhibitor monastrol was applied at 100 µM.

qRT-PCR

Levels of mRNA were monitored 48 hours after transfection with siRNAs in 12-well plates. HeLa cells were lysed using QIAshredder homogenizer (Qiagen). Total mRNA was extracted with RNeasy Mini Kit and RNase-Free DNase Set (Qiagen). Reverse transcription reactions were performed using 1 µg of total RNA, Superscript II Reverse Transcriptase (Invitrogen) and random primers (Microsynth). qRT-PCR was performed using target-specific oligonucleotide primers and LightCycler 480 SYBR Green I Master (Roche) on a Light Cycler 480 System (Roche). Primers were designed using appropriate parameters (MacVector) and the sequences are available upon request. Downregulation efficiency was assessed by importing raw *Ct* values into Excel (Microsoft) and by calculating the mRNA level for each target relative to *GAPDH* mRNA. All experiments were performed in triplicate.

Immunofluorescence microscopy

Cells were fixed at room temperature for 8 minutes in 20 mM PIPES (pH 6.8), 10 mM EGTA, 1 mM $MgCl_2$, 0.2% Triton X-100, 4% formaldehyde. For cold-stable assays, cells were incubated in ice-cold medium for 15 or 7 minutes before fixation. The following primary antibodies were used: rabbit anti-CENP-O (1:500) (McAinsh et al., 2006), mouse anti-α-tubulin (1:10,000; Sigma-Aldrich), rabbit anti-α-tubulin (1:1000; Abcam), mouse anti-γ-tubulin (1:2000; Sigma), CREST antisera (1:400; Antibodies Incorporated), rabbit anti-CENP-L (1:250) (Amaro et al., 2010), rabbit anti-Nnf1R (1:2000) (McAinsh et al., 2006), rabbit anti-MCAK (1:2000) (Amaro et al., 2010), mouse anti-Ndc80 (1:2000; Abcam), mouse-anti dynein intermediate chain (1:200; Sigma), rabbit anti-CENP-I (1:2000) (McClelland et al., 2007), rabbit anti-CENP-E (1:2000) (Meraldi et al., 2004) and rabbit anti-Aurora B (1:1000) (McClelland et al., 2007). Cross-adsorbed secondary antibodies were used (Invitrogen). 3D image stacks of mitotic cells were acquired in 0.2-µm steps using a 60× oil NA 1.4 objective or a 100× oil NA 1.4 objective on an Olympus DeltaVision microscope (Applied Precision, LLC) equipped with a DAPI-FITC-Rhod/TRCY5 filter set (Chroma) and a CoolSNAP HQ camera (Roper Scientific). The 3D image stacks were deconvolved with SoftWorx (Applied Precision, LLC) and mounted in figures using Photoshop and Illustrator (Adobe). For quantitative measurements of kinetochore protein levels, signals were determined and quantified with SoftWorx and IMARIS as described (McClelland et al., 2007). To measure the intensity of the k-fiber microtubules in cold-stable assays, the 3D images stacks acquired with Softworx were transferred to IMARIS (Bitplane) and subjected to spot detection in the CREST channel with a minimal spot size of 0.7 µm to detect kinetochores. Wrongly assigned spots (~1%) were manually curated. The mean intensity of tubulin signal was then calculated inside each 0.7-µm kinetochore sphere and corrected for background using the average tubulin intensity of 25 0.7-µm spheres placed outside of the mitotic spindle. For each independent experiment, the mean of the distribution in cells treated with control (scrambled) siRNA was normalized to 1. To measure the angle between spindle poles and sister-kinetochore pairs, the 3D stacks of Softworx images of stained HeLa EGFP–CENP-A/EGFP–centrin1 cells were exported to IMARIS, the spindle poles (center of spindle poles or the center of both spindle poles in the case of monastrol-treated cells) and individual sister-kinetochores were manually assigned and the positions exported to MATLAB to calculate the angle between the vector connecting both sister-kinetochores and the vector connecting the center of the spindle pole(s) and the center of each sister-kinetochore pair. The different angles were then plotted as a distribution diagram in MATLAB.

Live-cell imaging and photoactivation experiments

Live-cell imaging experiments of HeLa H2B–mCherry/mEGFP–α-tubulin or PA-GFP–α-tubulin/H2B–mRFP cells were performed at 37℃ in Lab-Tek II chambers (ThermoFisher Scientific) with Leibovitz L-15 medium containing 10% FCS.

HeLa H2B–mCherry/EGFP–α-tubulin cells were recorded every 3 minutes as 3D image stacks (eight stacks with 2-µm steps using a 40× oil NA 1.3 objective, or 12 stacks with 1-µm steps using a 60× oil NA 1.4 objective) on an Olympus DeltaVision microscope equipped with a EGFP/mRFP filter set (Chroma) and a CoolSNAP HQ camera. For photoactivation experiments, we identified the bipolar metaphase spindles with the H2B–mRFP signal and activated PA-GFP–α-tubulin in thin stripes (140 nm wide, as long as the metaphase plate) just above the metaphase plate using 100 iterations from a 405 nm laser (100%) on a Zeiss LSM 710-FCS confocal microscope. Fluorescence images were captured every 6.5 seconds for 325 seconds using a 40× water NA 1.2 objective. The progression of the photoactivation band towards the spindle pole, which corresponds to the poleward microtubule flux rate was manually measured in ImageJ (NIH, Bethesda, MD). The fluorescence intensities were quantified in ImageJ over the first 160 seconds of each movie (based on the average of six high signals on different k-fibers in each cell). Background spindle signal was subtracted for each time frame by measuring the same pixel area on the opposite side of the photoactivated spindle. Cells that underwent anaphase in this period were discarded, ensuring that all measurements were taken from cells in metaphase. The values were corrected for photobleaching by determining the percentage of fluorescence loss during the first 160 seconds in activated cells treated with 10 µM Taxol (based on the average of ten cells). The average data were fitted to a double-exponential curve $I=P_{fast}\exp(-k_{fast}t)+P_{slow}\exp(-k_{slow}t)$, where I is the proportion of the initial fluorescence intensity, P is the proportion of fluorescence decay due to the fast or slow process, k is the rate constant for fluorescence decay of the fast or slow process and t is time. Curve fitting was performed with MATLAB. The initial parameters P_{fast}, k_{fast}, P_{slow} and k_{slow} were set to 1, 0.1, 0.2 and 3.3×10^{-3}, respectively, on the basis of previous results (Amaro et al., 2010). The turnover half-time ($t_{1/2}$) for each process was calculated as $\ln2/k$ for each fast and slow process.

Kinetochore tracking assay

For the kinetochore tracking experiments, fluorescence time-lapse imaging of an EGFP–CENP-A cell line in LabTek II chambers at 37℃ was recorded with a 100× NA 1.4 objective on an Olympus DeltaVision microscope equipped with a CoolSNAP HQ2 camera and a EGFP/mRFP filter set at a temporal resolution of 7.5 seconds. Kinetochore tracking assay analysis yielded the trajectories for sister-kinetochore pairs (Jaqaman et al., 2010). The tracking software was applied to a minimum of 48 cells with a minimum of 1850 sister-kinetochore pairs per condition. The position of the sister-kinetochore pairs at each time point revealed the distribution of interkinetochore distances. In addition, for each time-lapse movie, the position of the metaphase plate was estimated by fitting a plane to the calculated kinetochore positions. To characterize the dynamics of individual sister-kinetochore pairs located on the metaphase plate over time, we followed the sister-kinetochore center position along the normal to the metaphase plate (spindle axis). The autocorrelation function of sister-kinetochore movements along the spindle axis yielded the periodicity of sister-kinetochore oscillations. The average speed of sister-kinetochores along the spindle axis was calculated as the standard deviation of the distribution of all sister-kinetochore frame-to-frame displacements. The metaphase plate thickness was calculated as the standard deviation of the distribution of aligned sister center positions along the normal to the metaphase plate.

Immunoblotting

Whole-cell lysate preparation and immunoblotting were carried out as described (McAinsh et al., 2006) using mouse anti-α-tubulin (1:10,000; Sigma-Aldrich), rabbit anti-Mad2 (1:500; Bethyl Antibodies) and rabbit anti-CENP-L antibodies (1:300) and anti-mouse or anti-rabbit horse-radish-peroxidase-conjugated secondary antibodies (Amersham).

Acknowledgements

We thank the ETH Light Microscopy Centre for microscopy support, Alexey Khodjakov, Matthew Good, Valentin Magidson and Reza Vafabakhsh for the joint development of the angle measurement code during the Physiology course at the Marine Biology Laboratory (Woods Hole, MA), Erich Nigg (University of Basel, CH) for sharing unpublished results on the CENP-O off-target effect, Daniel Gerlich (ETH Zurich, CH) for the H2B–mCherry/α-tubulin–mEGFP cell line, and Andrew McAinsh, Rob Cross (University of Warwick, UK) and members of the Meraldi laboratory for helpful discussions.

Funding

Work in the Meraldi laboratory is supported by an SNF-Förderungprofessur, a European Young Investigator (EURYI) award and the Eidgenössische Technische Hochschule (ETH) Zurich. J.M. is supported by a Marie Curie Intra-European Fellowship and an ETH Zurich Postdoctoral Fellowship. N.M. is a member of the Life Science Zurich Graduate School in Molecular Life Sciences.

Supplementary material available online at
http://jcs.biologists.org/lookup/suppl/doi:10.1242/jcs.091967/-/DC1

References

Amaro, A. C., Samora, C. P., Holtackers, R., Wang, E., Kingston, I. J., Alonso, M., Lampson, M., McAinsh, A. D. and Meraldi, P. (2010). Molecular control of kinetochore-microtubule dynamics and chromosome oscillations. *Nat. Cell Biol.* **12**, 319-329.

Aubin, J. E., Osborn, M. and Weber, K. (1980). Variations in the distribution and migration of centriole duplexes in mitotic PtK2 cells studied by immunofluorescence microscopy. *J. Cell Sci.* **43**, 177-194.

Bahe, S., Stierhof, Y. D., Wilkinson, C. J., Leiss, F. and Nigg, E. A. (2005). Rootletin forms centriole-associated filaments and functions in centrosome cohesion. *J. Cell Biol.* **171**, 27-33.

Bakhoum, S. F., Genovese, G. and Compton, D. A. (2009). Deviant kinetochore microtubule dynamics underlie chromosomal instability. *Curr. Biol.* **19**, 1937-1942.

Cai, S., O'Connell, C. B., Khodjakov, A. and Walczak, C. E. (2009). Chromosome congression in the absence of kinetochore fibres. *Nat. Cell Biol.* **11**, 832-838.

Carroll, C. W., Silva, M. C., Godek, K. M., Jansen, L. E. and Straight, A. F. (2009). Centromere assembly requires the direct recognition of CENP-A nucleosomes by CENP-N. *Nat. Cell Biol.* **11**, 896-902.

Cheeseman, I. M. and Desai, A. (2008). Molecular architecture of the kinetochore-microtubule interface. *Nat. Rev. Mol. Cell Biol.* **9**, 33-46.

Cimini, D., Howell, B., Maddox, P., Khodjakov, A., Degrassi, F. and Salmon, E. D. (2001). Merotelic kinetochore orientation is a major mechanism of aneuploidy in mitotic mammalian tissue cells. *J. Cell Biol.* **153**, 517-527.

Cimini, D., Moree, B., Canman, J. C. and Salmon, E. D. (2003). Merotelic kinetochore orientation occurs frequently during early mitosis in mammalian tissue cells and error correction is achieved by two different mechanisms. *J. Cell Sci.* **116**, 4213-4225.

DeLuca, J. G., Moree, B., Hickey, J. M., Kilmartin, J. V. and Salmon, E. D. (2002). hNuf2 inhibition blocks stable kinetochore-microtubule attachment and induces mitotic cell death in HeLa cells. *J. Cell Biol.* **159**, 549-555.

DeLuca, J. G., Gall, W. E., Ciferri, C., Cimini, D., Musacchio, A. and Salmon, E. D. (2006). Kinetochore microtubule dynamics and attachment stability are regulated by Hec1. *Cell* **127**, 969-982.

Elbashir, S. M., Harborth, J., Lendeckel, W., Yalcin, A., Weber, K. and Tuschl, T. (2001). Duplexes of 21-nucleotide RNAs mediate RNA interference in cultured mammalian cells. *Nature* **411**, 494-498.

Ganem, N. J. and Compton, D. A. (2004). The KinI kinesin Kif2a is required for bipolar spindle assembly through a functional relationship with MCAK. *J. Cell Biol.* **166**, 473-478.

Ganem, N. J., Godinho, S. A. and Pellman, D. (2009). A mechanism linking extra centrosomes to chromosomal instability. *Nature* **460**, 278-282.

Hauf, S., Cole, R. W., LaTerra, S., Zimmer, C., Schnapp, G., Walter, R., Heckel, A., van Meel, J., Rieder, C. L. and Peters, J. M. (2003). The small molecule Hesperadin reveals a role for Aurora B in correcting kinetochore-microtubule attachment and in maintaining the spindle assembly checkpoint. *J. Cell Biol.* **161**, 281-294.

Hori, T., Amano, M., Suzuki, A., Backer, C. B., Welburn, J. P., Dong, Y., McEwen, B. F., Shang, W. H., Suzuki, E., Okawa, K. et al. (2008). CCAN makes multiple contacts with centromeric DNA to provide distinct pathways to the outer kinetochore. *Cell* **135**, 1039-1052.

Hua, S., Wang, Z., Jiang, K., Huang, Y., Ward, T., Zhao, L., Dou, Z. and Yao, X. (2011). CENP-U cooperates with Hec1 to orchestrate kinetochore-microtubule attachment. *J. Biol. Chem.* **286**, 1627-1638.

Hubner, N. C., Wang, L. H., Kaulich, M., Descombes, P., Poser, I. and Nigg, E. A. (2010). Re-examination of siRNA specificity questions role of PICH and Tao1 in the spindle checkpoint and identifies Mad2 as a sensitive target for small RNAs. *Chromosoma* **119**, 149-165.

Jaqaman, K., King, E. M., Amaro, A. C., Winter, J. R., Dorn, J. F., Elliott, H. L., McHedlishvili, N., McClelland, S. E., Porter, I. M., Posch, M. et al. (2010). Kinetochore alignment within the metaphase plate is regulated by centromere stiffness and microtubule depolymerases. *J. Cell Biol.* **188**, 665-679.

Kapoor, T. M., Lampson, M. A., Hergert, P., Cameron, L., Cimini, D., Salmon, E. D., McEwen, B. F. and Khodjakov, A. (2006). Chromosomes can congress to the metaphase plate before biorientation. *Science* **311**, 388-391.

Kline-Smith, S. L., Khodjakov, A., Hergert, P. and Walczak, C. E. (2004). Depletion of centromeric MCAK leads to chromosome congression and segregation defects due to improper kinetochore attachments. *Mol. Biol. Cell* **15**, 1146-1159.

Knowlton, A. L., Lan, W. and Stukenberg, P. T. (2006). Aurora B is enriched at merotelic attachment sites, where it regulates MCAK. *Curr. Biol.* **16**, 1705-1710.

Kops, G. J., Saurin, A. T. and Meraldi, P. (2010). Finding the middle ground: how kinetochores power chromosome congression. *Cell. Mol. Life Sci.* **67**, 2145-2161.

Kwok, B. H. and Kapoor, T. M. (2007). Microtubule flux: drivers wanted. *Curr. Opin. Cell Biol.* **19**, 36-42.

Lampson, M. A., Renduchitala, K., Khodjakov, A. and Kapoor, T. M. (2004). Correcting improper chromosome-spindle attachments during cell division. *Nat. Cell Biol.* **6**, 232-237.

Lan, W., Zhang, X., Kline-Smith, S. L., Rosasco, S. E., Barrett-Wilt, G. A., Shabanowitz, J., Hunt, D. F., Walczak, C. E. and Stukenberg, P. T. (2004). Aurora B phosphorylates centromeric MCAK and regulates its localization and microtubule depolymerization activity. *Curr. Biol.* **14**, 273-286.

Maffini, S., Maia, A. R., Manning, A. L., Maliga, Z., Pereira, A. L., Junqueira, M., Shevchenko, A., Hyman, A., Yates, J. R., 3rd, Galjart, N. et al. (2009). Motor-independent targeting of CLASPs to kinetochores by CENP-E promotes microtubule turnover and poleward flux. *Curr. Biol.* **19**, 1566-1572.

Maiato, H., Fairley, E. A., Rieder, C. L., Swedlow, J. R., Sunkel, C. E. and Earnshaw, W. C. (2003). Human CLASP1 is an outer kinetochore component that regulates spindle microtubule dynamics. *Cell* **113**, 891-904.

Manning, A. L., Bakhoum, S. F., Maffini, S., Correia-Melo, C., Maiato, H. and Compton, D. A. (2010). CLASP1, astrin and Kif2b form a molecular switch that regulates kinetochore-microtubule dynamics to promote mitotic progression and fidelity. *EMBO J.* **29**, 3531-3543.

McAinsh, A. D., Meraldi, P., Draviam, V. M., Toso, A. and Sorger, P. K. (2006). The human kinetochore proteins Nnf1R and Mcm21R are required for accurate chromosome segregation. *EMBO J.* **25**, 4033-4049.

McClelland, S. E., Borusu, S., Amaro, A. C., Winter, J. R., Belwal, M., McAinsh, A. D. and Meraldi, P. (2007). The CENP-A NAC/CAD kinetochore complex controls chromosome congression and spindle bipolarity. *EMBO J.* **26**, 5033-5047.

Meraldi, P., Draviam, V. M. and Sorger, P. K. (2004). Timing and checkpoints in the regulation of mitotic progression. *Dev. Cell* **7**, 45-60.

Moroi, Y., Peebles, C., Fritzler, M. J., Steigerwald, J. and Tan, E. M. (1980). Autoantibody to centromere (kinetochore) in scleroderma sera. *Proc. Natl. Acad. Sci. USA* **77**, 1627-1631.

Okada, M., Cheeseman, I. M., Hori, T., Okawa, K., McLeod, I. X., Yates, J. R., Desai, A. and Fukagawa, T. (2006). The CENP-H-I complex is required for the efficient incorporation of newly synthesized CENP-A into centromeres. *Nat. Cell Biol.* **8**, 446-457.

Rattner, J. B. and Berns, M. W. (1976). Centriole behavior in early mitosis of rat kangaroo cells (PTK2). *Chromosoma* **54**, 387-395.

Rieder, C. L., Davison, E. A., Jensen, L. C., Cassimeris, L. and Salmon, E. D. (1986). Oscillatory movements of monooriented chromosomes and their position relative to the spindle pole result from the ejection properties of the aster and half-spindle. *J. Cell Biol.* **103**, 581-591.

Rosenblatt, J. (2005). Spindle assembly: asters part their separate ways. *Nat. Cell Biol.* **7**, 219-222.

Rosenblatt, J., Cramer, L. P., Baum, B. and McGee, K. M. (2004). Myosin II-dependent cortical movement is required for centrosome separation and positioning during mitotic spindle assembly. *Cell* **117**, 361-372.

Salmon, E. D. and Begg, D. A. (1980). Functional implications of cold-stable microtubules in kinetochore fibers of insect spermatocytes during anaphase. *J. Cell Biol.* **85**, 853-865.

Schaar, B. T., Chan, G. K., Maddox, P., Salmon, E. D. and Yen, T. J. (1997). CENP-E function at kinetochores is essential for chromosome alignment. *J. Cell Biol.* **139**, 1373-1382.

Schmidt, J. C., Kiyomitsu, T., Hori, T., Backer, C. B., Fukagawa, T. and Cheeseman, I. M. (2010). Aurora B kinase controls the targeting of the Astrin-SKAP complex to bioriented kinetochores. *J. Cell Biol.* **191**, 269-280.

Silk, A. D., Holland, A. J. and Cleveland, D. W. (2009). Requirements for NuMA in maintenance and establishment of mammalian spindle poles. *J. Cell Biol.* **184**, 677-690.

Silkworth, W. T., Nardi, I. K., Scholl, L. M. and Cimini, D. (2009). Multipolar spindle pole coalescence is a major source of kinetochore mis-attachment and chromosome mis-segregation in cancer cells. *PLoS ONE* **4**, e6564.

Steigemann, P., Wurzenberger, C., Schmitz, M. H., Held, M., Guizetti, J., Maar, S. and Gerlich, D. W. (2009). Aurora B-mediated abscission checkpoint protects against tetraploidization. *Cell* **136**, 473-484.

Stumpff, J., von Dassow, G., Wagenbach, M., Asbury, C. and Wordeman, L. (2008). The kinesin-8 motor Kif18A suppresses kinetochore movements to control mitotic chromosome alignment. *Dev. Cell* **14**, 252-262.

Tanaka, T. U., Rachidi, N., Janke, C., Pereira, G., Galova, M., Schiebel, E., Stark, M. J. and Nasmyth, K. (2002). Evidence that the Ipl1-Sli15 (Aurora kinase-INCENP) complex promotes chromosome bi-orientation by altering kinetochore-spindle pole connections. *Cell* **108**, 317-329.

Tanenbaum, M. E. and Medema, R. H. (2010). Mechanisms of centrosome separation and bipolar spindle assembly. *Dev. Cell* **19**, 797-806.

Toso, A., Winter, J. R., Garrod, A. J., Amaro, A. C., Meraldi, P. and McAinsh, A. D. (2009). Kinetochore-generated pushing forces separate centrosomes during bipolar spindle assembly. *J. Cell Biol.* **184**, 365-372.

Walczak, C. E. and Heald, R. (2008). Mechanisms of mitotic spindle assembly and function. *Int. Rev. Cytol.* **265**, 111-158.

Waters, J. C., Cole, R. W. and Rieder, C. L. (1993). The force-producing mechanism for centrosome separation during spindle formation in vertebrates is intrinsic to each aster. *J. Cell Biol.* **122**, 361-372.

Westhorpe, F. G., Diez, M. A., Gurden, M. D., Tighe, A. and Taylor, S. S. (2010). Re-evaluating the role of Tao1 in the spindle checkpoint. *Chromosoma* **119**, 371-379.

Wood, K. W., Sakowicz, R., Goldstein, L. S. and Cleveland, D. W. (1997). CENP-E is a plus end-directed kinetochore motor required for metaphase chromosome alignment. *Cell* **91**, 357-366.

Yang, J., Gao, J., Adamian, M., Wen, X. H., Pawlyk, B., Zhang, L., Sanderson, M. J., Zuo, J., Makino, C. L. and Li, T. (2005). The ciliary rootlet maintains long-term stability of sensory cilia. *Mol. Cell. Biol.* **25**, 4129-4137.

Zhai, Y., Kronebusch, P. J. and Borisy, G. G. (1995). Kinetochore microtubule dynamics and the metaphase-anaphase transition. *J. Cell Biol.* **131**, 721-734.